Journal of Innate Immunity

Research Article

J Innate Immun 2022;14:657–672
DOI: 10.1159/000524561

Received: January 27, 2022
Accepted: March 18, 2022
Published online: May 5, 2022

HMGB1-Like Dorsal Switch Protein 1 Triggers a Damage Signal in Mosquito Gut to Activate Dual Oxidase via Eicosanoids

Shabbir Ahmed Seyedeh Minoo Sajjadian Yonggyun Kim

Department of Plant Medicals, Andong National University, Andong, South Korea

Keywords
Dual oxidase · Dorsal switch protein 1 · Eicosanoids · Reactive oxygen species · *Aedes albopictus*

Abstract
Several mosquitoes transmit human pathogens by blood feeding, with the gut being the main entrance for the pathogens. Thus, the gut epithelium defends the pathogens by eliciting potent immune responses. However, it was unclear how the mosquito gut discriminates pathogens among various microflora in the lumen. This study proposed a hypothesis that a damage signal might be specifically induced by pathogens in the gut. The Asian tiger mosquito, *Aedes albopictus*, encodes dorsal switch protein 1 (*Aa-DSP1*) as a putative damage-associated molecular pattern (DAMP). Aa-DSP1 was localized in the nucleus of the midgut epithelium in naïve larvae. Upon infection by a pathogenic bacterium, *Serratia marcescens*, Aa-DSP1 was released to hemocoel and activated phospholipase A_2 (PLA_2). The activated PLA_2 increased the level of prostaglandin E_2 (PGE_2) in the gut and subsequently increased Ca^{2+} signal to produce reactive oxygen species (ROS) via dual oxidase (Duox). Inhibition of Aa-DSP1 via RNA interference or specific inhibitor treatment failed to increase PGE_2/Ca^{2+} signal upon the bacterial infection. Thus, the inhibitors specifically targeting eicosanoid biosynthesis significantly prevented the upregulation of ROS production in the gut and enhanced mosquito mortality after the bacterial infection. However, such inhibitory effects were rescued by adding PGE_2. These suggest that Aa-DSP1 plays an important role in immune response of the mosquito gut as a DAMP during pathogen infection by triggering a signaling pathway, DSP1/PLA_2/Ca^{2+}/Duox.

Introduction

Mosquitoes can transmit a wide range of pathogens that can cause diseases such as malaria, dengue, yellow fever, and Zika known to have a devastating impact on human health [1]. Although the use of insecticides for mosquitoes is a major tool for disease control, intensive use of insecticides leads to unexpected adverse outcomes such as environmental pollutants threatening human/wildlife health and development of insecticide resistance [2, 3]. Thus, alternative tools for mosquito control are urgently needed [4].

Karger@karger.com
www.karger.com/jin

Correspondence to:
Yonggyun Kim, hosanna@anu.ac.kr

The Asian tiger mosquito, *Aedes albopictus*, was indigenous to tropical and subtropical areas of Asia. However, it is now regarded as one of the most rapidly spreading species in the world [1, 5]. As a capable vector, it can transmit at least 22 arboviruses including Chikungunya, Dengue, and Zika viruses, resulting in severe outbreaks worldwide [6].

Various microbes threaten mosquito survival in wildlife. Especially, the digestive tract of a mosquito is exposed to these microbes when ingesting diets. Although beneficial microbes are required for mosquito development, pathogens should be removed by gut immunity. To regulate gut immunity in a broad sense, two isoforms of a transcriptional factor, Nubbin, which is a homeodomain protein, antagonistically regulate the expression of immune-associated genes in the *Drosophila* midgut by inducing the gene expression and suppressing excessive expressions [7]. Among these immune-associated molecules, antimicrobial peptides (AMPs) and reactive oxygen species (ROS) act as two main immune effectors in the insect gut [8, 9]. AMPs play a crucial role in maintaining homeostatic microbial flora in the gut by regulating the growth of commensal microbes [10]. Upon pathogenic microbial infection, the midgut produces ROS to remove pathogens [11]. However, ROS and AMPs might have harmful effects on host insects and/or symbiotic microbes, and so their production should be tightly regulated [12].

ROS in the midgut is produced by dual oxidase (Duox) [13]. Duox contains a Ca^{2+}-binding EF domain. Its enzyme activity is induced by Ca^{2+} to produce ROS [14]. Thus, regulating ROS production can be achieved by regulating Duox activity. One regulator of Duox has been identified to be uracil released from bacterial pathogens in *Drosophila*, in which uracil acts as a pathogen-specific molecule that enables the host to distinguish uracil-releasing microorganisms as pathogens from no uracil-releasing commensals or symbionts in the gut mucosal epithelium [15]. The binding of uracil to an unidentified receptor on the midgut epithelial membrane can trigger the PLCβ/PKC/Ca^{2+} signal pathway to activate Duox [9]. In contrast, Duox is activated by eicosanoids in other insects such as two lepidopterans, *Spodoptera exigua* [16] and *Plutella xylostella* [17], in which inhibition of eicosanoid biosynthesis prevents ROS production in the midgut upon pathogen infection. These suggest that eicosanoids play a crucial role in gut immunity by activating Duox in insects, including *A. albopictus*.

Eicosanoids are a group of oxygenated C20 polyunsaturated fatty acids that can mediate various physiological processes including immune responses in metazoan animals [18]. Eicosanoid production is initiated by the release of free C20 polyunsaturated fatty acids from phospholipids due to the catalytic activity of phospholipase A_2 (PLA_2) [19]. Among eicosanoids, prostaglandins (PGs) play a crucial role in mediating various immune responses in mosquito midgut [20]. Several PGs along with prostaglandin E_2 (PGE_2) receptor and its downstream signal components found in *S. exigua* can mediate the induction of intracellular Ca^{2+} levels [21]. Thus, eicosanoids may mediate ROS production in *A. albopictus* by elevating Ca^{2+} levels.

A question is raised on how mosquito gut can discriminate pathogenic microbes from various gut microflora. We propose in this study that a novel insect damage-associated molecular pattern (DAMP) in mosquitoes might trigger gut immunity upon pathogen infection. Dorsal switch protein 1 (DSP1) is known as an insect DAMP molecule [22]. DSP1 is an orthologue of vertebrate high mobility group B1 (HMGB1) [23]. HMGB1 is a ubiquitously expressed and highly conserved nuclear protein that plays an important role in chromatin organization and transcriptional regulation in plants and animals [24]. Under stress conditions including pathogen infection, HMGB1 is released to act as a DAMP to activate the innate immune system by interacting with pattern recognition receptors (PRRs) [25]. Insect DSP1 can act as a transcription factor and a chromatin remodeling factor [23, 26]. In *S. exigua* infected by entomopathogenic bacteria, DSP1 is released from the fat body. It then activates PLA_2 to elevate eicosanoids known to mediate cellular and humoral immune responses [22]. DSP1 of *Tenebrio molitor*, a coleopteran insect, can also mediate immune responses to bacterial infection [27]. Thus, we hypothesized that DSP1 in the mosquito midgut might act as a DAMP against pathogen infection. We also hypothesized that DSP1 could activate eicosanoid biosynthesis to mediate various immune responses along with Duox activation to produce ROS in the mosquito gut lumen.

Materials and Methods

Mosquito Rearing, Bacterial Infection, and Tissue Preparation

Aedes albopictus mosquitoes were reared at 28°C with a relative humidity of 70 ± 5% under a 12 h/12 h day-night cycle. During adult stages, mosquitoes were maintained with 10% (wt/vol) sucrose solution. Two-day-old mosquitoes were fed on blood for oviposition. Larvae were reared on groundfish food supplements under the same rearing conditions. Under these conditions, *A. albopictus* underwent four larval instars (L1–L4) before pupation.

For bacterial infection, *Serratia marcescens*, a gram-negative bacterium, was cultured with a nutrient broth medium for 20 h at 28°C in a shaking (200 rpm) incubator. After centrifuging the culture at 8,000 *g* for 20 min, cells were washed with sterile water and used for immune challenge through a feeding assay. For oral infection of larval stages, *S. marcescens* (Sm) was added to the water at a final concentration of 10^4 CFU/mL.

For tissue preparation, whole alimentary canals were isolated from larval instars (L3–L4), pupae (2–3 days old), and adults (2–3 days old). In the case of L1–L2 larvae, the whole body was used. To prepare tissue samples, 50 L1–L2, 30 L3–L4 larvae, pupae, and adults were used.

Chemicals and Their Application

Arachidonic acid (AA: 5,8,11,14-eicosatetraenoic acid), dexamethasone [DEX (11β, 16α)-9-fluoro-11,17,21-trihydroxy-16-methylpregna-1,4-diene-3], naproxen [NAP (*S*)-(+)-2-(6-methoxy-2-naphthyl)propionic acid], esculetin (ESC: 6-hydroxy-7-methoxycoumarin), 3-ethoxy-4-methoxyphenol (EMP) as a specific inhibitor to DSP1 [22], and PGE_2 ((5*Z*,11α,13*E*,15*S*)-11,15-dihydroxy-9-oxoprosta-5,13-dienoic acid) were purchased from Sigma-Aldrich Korea (Seoul, Korea) and leukotriene B_4 (LTB_4: 5*S*,12*R*-dihydroxy-6*Z*,8*E*,10*E*,14*Z*-eicosatetraenoic acid) was purchased from Cayman Chemicals (Ann Arbor, MI, USA). These chemicals were supplied in acetone, ethanol, or powder form. Chemicals in powder form were directly dissolved in dimethyl sulfoxide (DMSO) and stock concentrations (100 μg/μL or 10^5 ppm) were prepared. In case of chemicals in acetone or ethanol, they were dried with nitrogen gas under a fume hood and then prepared in stock concentrations (100 μg/μL or 10^5 ppm) with DMSO. Finally, a working solution (1,000 ppm) was prepared by a serial dilution using DMSO. Fura-8AM was purchased from AAT Bioquest (Sunnyvale, CA, USA) and dissolved in DMSO. Phosphate-buffered saline (PBS) was prepared with 100 mM phosphoric acid and adjusted to pH 7.4.

Bioinformatics

In the present study, *A. albopictus* Duox (*Aa-Duox*; GenBank accession number: XM_020077353.2) and DSP1 (*Aa-DSP1*; GenBank accession number: XP_019544674.2) were used. Protein domain structure was predicted using HMMER (https://www.ebi.ac.uk) and Pfam (http://pfam.xfam.org). Phylogenetic analyses and phylogenetic tree construction with the Neighbor-joining method were performed using MEGA6 and ClustalW programs, respectively. Bootstrapping values were obtained with 1,000 repetitions to support branching and clustering.

RNA Extraction and RT-qPCR

Total RNAs were extracted from all developmental stages of *A. albopictus* using Trizol reagent (Invitrogen, Carlsbad, CA, USA) according to the manufacturer's instruction. To extract RNAs from whole bodies of *A. albopictus* at different developmental stages, >200 eggs, 50 L1–L2, 10 L3–L4, 5 pupa, and five adults were used. Different tissue samples (fat body, midgut, and epidermis) were isolated from 50 L4 larvae. Extracted RNAs were dissolved in 50 μL diethyl pyrocarbonate (DEPC)-treated deionized and distilled water. First-strand cDNA was synthesized from 1 μg of RNA using Maxime RT PreMix (Intron Biotechnology, Seoul, Korea) containing oligo dT primers according to the manufacturer's instruction. The synthesized cDNA was used as a template for PCR amplification or for constructing dsRNA. Real-time quantitative polymerase chain reaction (qPCR) was carried out in a reaction volume of 20 μL using 2× SYBR Green Realtime PCR Master Mix (Toyobo, Osaka, Japan), 5 mM of gene-specific forward and reverse primers, and 80 ng cDNA as template. PCR amplification was performed at 95°C for 10 min for initial heat treatment, followed by 40 cycles of 98°C for 30 s, 52°C (*Aa-Duox*) or 55°C (*Aa-DSP1*) for 30 s, and 72°C for 30 s. It was then finished with a final extension step at 72°C for 7 min. Melting curves of products were obtained to confirm amplification specificity. For quantitative analysis and estimating mRNA expression levels of target genes with β-actin as a reference gene, the comparative C_T ($2^{-\Delta\Delta CT}$) method [28] was used. All experiments were independently replicated three times. All primer sequences used in this study for RT-PCR and RT-qPCR are presented in online supplementary Table S1 (see www.karger.com/doi/10.1159/000524561 for all online suppl. material).

dsRNA Preparation and RNAi

Double-stranded RNA (dsRNA) specific to *Aa-Duox* or *Aa-DSP1* was prepared as described in our previous study [16]. Briefly, a partial sequence was produced by PCR using gene-specific primers containing a T7 promoter sequence at the 5′ end (online suppl. Table S1). The PCR product was used as a template to generate dsRNA using a MEGAscript RNA interference (RNAi) kit (Ambion, Austin, TX, USA) according to the manufacturer's instruction. Sense and antisense-RNA strands were synthesized using T7 RNA polymerase at 37°C for 4 h. As control dsRNA (dsCON), a 500 bp fragment of the green fluorescent protein gene was synthesized [29]. The resulting dsRNA was purified and mixed with transfection reagent Metafectene PRO (Biontex, Planegg, Germany) at a ratio of 1:1 (vol/vol) and then incubated at 25°C for 30 min to form liposomes. Five microgram of dsRNA was added to 1 mL of water medium containing L4 larvae. At different time points post dsRNA treatment, RNAi efficacy was determined by RT-qPCR as described above. Each treatment was replicated three times.

ROS Measurement

An OxiSelect intracellular ROS assay kit (Cell Biolabs, San Diego, CA, USA) was used to quantify ROS levels in L4 larvae of *A. albopictus*. For measuring ROS levels in the gut lumen, gut content was collected by squeezing out the midgut and centrifuged at 1,000 *g* for 2 min. The supernatant was mixed with 0.1× DCFH-DA (dichlorofluorescein diacetate) at the same volume. After incubation at 37°C for 30 min, the reaction product (150 μL) was then transferred to a 96-well plate. Fluorescence was read at an emission wavelength of 530 nm after excitation at 480 nm. A calibration curve was drawn using serial dilutions of dichlorofluorescein standard in TC-100 cell culture medium. ROS levels were normalized to protein amounts [30]. At 12 h after bacterial and/or chemical treatment, ROS production was assessed. Each treatment was replicated three times with independent sample preparations using five larvae per replication.

Pathogenicity Test

Ten L2 larvae were added to each well of a 48-well plate. Chemicals including DEX, AA, NAP, ESC, PGE_2, EMP, and LTB_4 were dissolved in DMSO and added to larval water at a final concentration of 1,000 ppm. Mortality in the presence or absence of Sm (10^4 CFU/mL) was checked for 4 days. All experiments were performed using three independent biological replicates.

Secretory PLA_2 Activity

Secretory PLA_2 (sPLA_2) activity in the carcass (excluding gut) of L4 larva was fluorometrically determined using a commercial assay kit (sPLA_2 assay kit; Cayman Chemical, Ann Arbor, MI, USA) with diheptanoyl thio-phosphatidyl choline as an enzyme-substrate following the method described by Vatanparast et al. [29]. A spectrofluorometer (VICTOR multi-label Plate reader; PerkinElmer, Waltham, MA, USA) was used to measure enzyme activity. Changes in absorbance at 405 nm of the reaction product were measured and plotted to obtain the slope of a linear portion

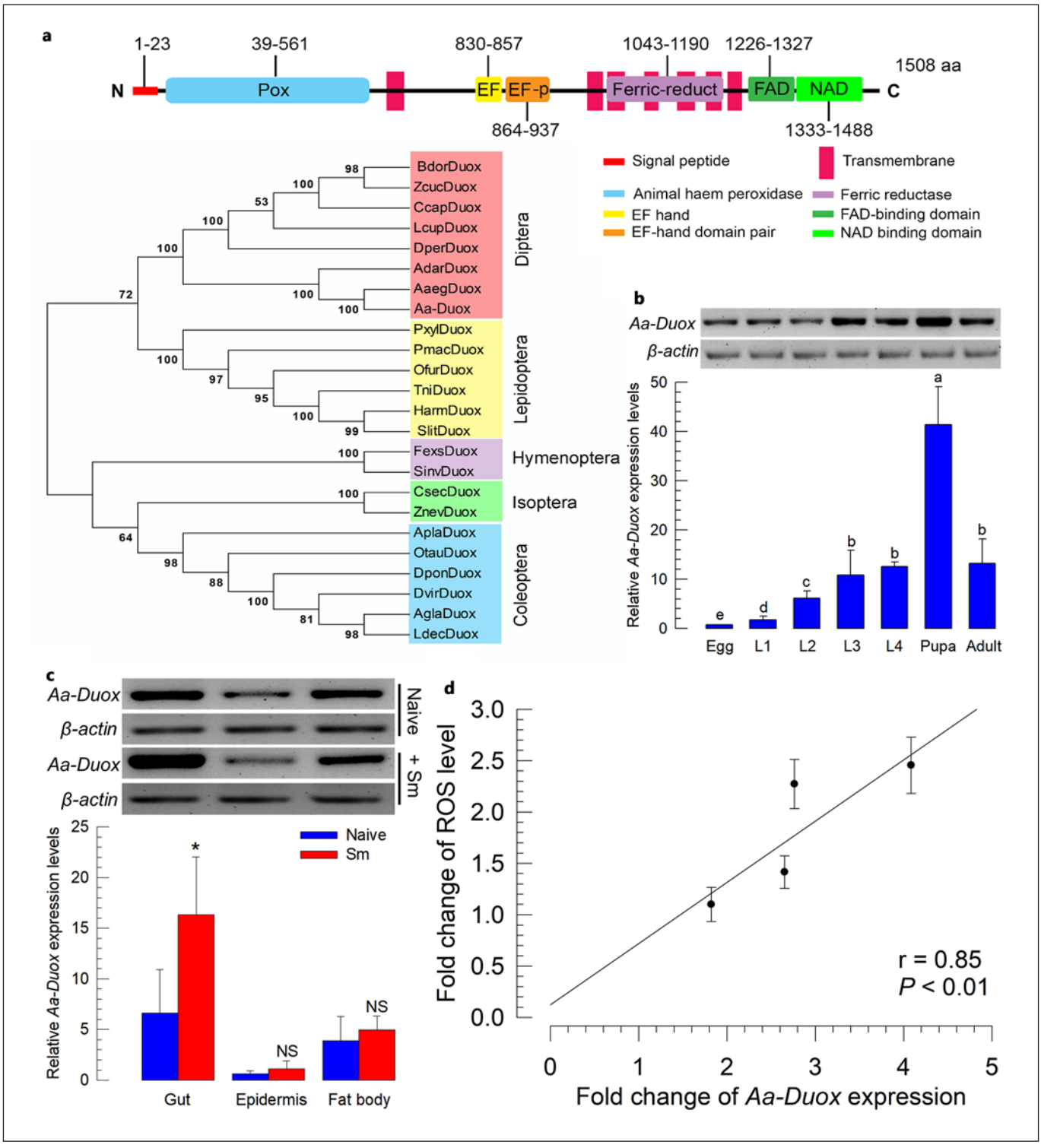

1

(For legend see next page.)

of the curve. Each treatment was replicated three times with independent sample preparations using five larvae per replication. Specific enzyme activity (μmol/min/μg) was calculated by dividing the absorbance change by the protein amount used as the enzyme source for the reaction.

Western Blotting

For a bacterial treatment with Sm, L4 larvae were fed with Sm (10^4 CFU/mL)-treated water for 12 h. For the inhibitory assay, EMP (1,000 ppm) was added along with Sm (10^4 CFU/mL). At 12 h posttreatment, for each sample preparation, the carcass (excluding gut) of 10 L4 larvae was collected carefully into PBS containing a protease inhibitor cocktail (Sigma-Aldrich, Korea) and 1 mM phenylmethylsulfonyl fluoride (Thermo Fisher Scientific, Korea). As we observed the elevated $sPLA_2$ activity at 12 postinfection, we selected this time point for DSP1 expression analysis. After centrifuging at 500 *g* for 5 min, the supernatant was collected and mixed with 4× denatured sample buffer (200 mM Tris-HCL, 400 mM DTT, 8% SDS, 0.4% bromophenol blue, and 40% glycerol). After 5 min of denaturation at 95°C, proteins (20 μg per sample) were separated on 10% SDS-PAGE at 95 V. Separated proteins from the gel were transferred onto nitrocellulose membranes (BioRad, Hercules, CA, USA) for 50 min at 95 V in chilled transfer buffer (25 mM Tris, 190 mM glycine, 20% methanol, pH 8.5). Membranes were briefly rinsed with Tris-buffered saline containing Tween-20 (TBST) (20 mM Tris, 150 mM NaCl, and 0.1% Tween 20, pH 7.5) and then blocked with 3% bovine serum albumin (BSA) in TBST at room temperature (RT) for 1 h. Membranes were then incubated with DSP1 antibody raised against Se-DSP1 in rabbit (Abclon, Seoul, Korea) diluted 5,000 times with TBST containing 3% BSA at 4°C overnight. After washing three times with TBST (10 min for each), the membrane was incubated with an anti-rabbit IgG-alkaline phosphatase secondary antibody (Sigma-Aldrich, Korea) at a dilution of 1:20,000 in TBST containing 3% BSA for 1 h at RT. Blots were rinsed three times with TBST. As a reference protein, α-tubulin was used. It was detected with a polyclonal antibody (GTX112141; GeneTex, Irvine, CA, USA) after dilution with TBST containing 3% BSA at 1:1,000. To detect alkaline phosphatase activity, nitrocellulose membrane blots were incubated with BCIP (5-bromo-4-chloro-3′-indolyphosphate *p*-toluidine salt)/NBT (nitro-blue tetrazolium chloride) (Sigma-Aldrich, Korea) as a substrate of alkaline phosphatase.

Immunofluorescence Assay

L4 larvae were fed with Sm (10^4)-treated water. After 12 h of feeding, the midgut was collected onto glass slides. After removing gut contents, TC100 insect tissue culture medium was added immediately, followed by incubation at RT in a wet chamber for 5 min. After removing the medium, the gut sample was then fixed with 4% formaldehyde for 20 min at RT. After the fixative was replaced with PBS, the midgut was incubated at RT for 10 min. After washing with PBS two more times, the midgut was permeabilized with 0.2% Triton X-100 in PBS for 20 min at RT. After washing with PBS three times, blocking was done with 5% skimmed milk powder in PBS at RT for 20 min. A DSP1 antibody [22] raised against Se-DSP1 in rabbit was added after it was diluted with 3% BSA in PBS (1:100) followed by incubation at RT for 1 h 20 min. After washing with PBS three times, the midgut was incubated with an anti-rabbit secondary antibody (Sigma-Aldrich, Korea) diluted with 3% BSA in PBS (1:5,000) for 1 h. After washing with PBS three times, midguts were incubated with 4′,6-diamidino-2-phenylindole (DAPI, 1 μg/mL) (Thermo Scientific, Korea) in PBS at RT for 5 min for nucleus staining. To detect PGE_2 level in the gut epithelium, 1% of PGE_2 antibody (ab2318; Abcam, Cambridge, UK) in PBS was used after blocking with 5% skimmed milk at RT for 2 h. After washing with PBS three times, gut samples were incubated with 1% anti-rabbit-FITC conjugated antibody (Thermo Fisher Scientific, Korea) in PBS at RT for 1 h. After washing with PBS three times, the nucleus was stained with DAPI (1 mg/mL) as described above. After washing with PBS three times and adding 50% glycerol, tissue samples were covered by cover glass and observed with a fluorescence microscope (DM2500; Leica, Wetzlar, Germany) at ×200 magnification. Fluorescence changes were analyzed using ImageJ software (https://imagej.nih.gov/ij). Each treatment was replicated three times, and each replication contained three larvae.

In vitro Ca^{2+} Signaling in Response to Sm Treatment

L4 larvae were challenged with Sm at 10^4 CFU/mL for 12 h. Midgut tissues of challenged larvae were dissected carefully into TC100 insect medium and incubated at RT in a wet chamber for 10 min. After removing TC100, midgut tissues were then incubated with 3 μL Fura-8AM (1 mM) at RT for another 10 min. After washing with PBS three times, midgut tissues were permeabilized with 0.2% Triton X-100 in PBS for 20 min at RT. Following washing with PBS three times, the midgut was incubated with DAPI (1 μg/mL) in PBS at RT for 5 min to stain the nucleus. Finally, the midgut was washed with PBS three times and fixed with 50% glycerol. Fura signals in the midgut were observed under a fluorescence microscope (DM500; Leica, Wetzlar, Germany) at ×200 magnification. Fluorescence changes were analyzed using ImageJ software (https://imagej.nih.gov/ij). Each treatment was replicated three times, and each replication contained three larvae.

Fig. 1. Molecular characterization of *Aa-Duox*. **a** Functional domain and phylogenetic analyses of *Aa-Duox*. Domains were predicted using HMMER (https://www.ebi.ac.uk) and Pfam (http://pfam.xfam.org). Predicted domains included "Pox" for peroxidase, "EF" for calcium-binding EF-hand, "TM" for transmembrane, "Ferric-reduct" for ferric chelate reductase, "FAD" for FAD-binding domain, and "NAD" for NAD-binding domain. The tree was generated by the Neighbor-joining method using MEGA 6.0. Bootstrapping values were obtained with 1,000 repetitions to support branch and clustering. Amino acid sequences were retrieved from GenBank. Accession numbers of genes are shown in online supplementary Table S2. **b** Expression profile of *Aa-Duox*. Expression patterns in different developmental stages: egg, first to fourth-instar larvae ("L1–L4"), pupa, and adult. **c** Expression patterns and induction of *Aa-Duox* expression in response to bacterial challenge in indicated tissues of L4 larvae, including midgut ("Gut"), epidermis, and fat body. L4 larvae were treated with Sm (10^4 CFU/mL) through the feeding assay for 12 h and dissected for studying expression patterns. **d** Correlation between *Aa-Duox* expression and ROS production in the midgut of L4 larvae. β-Actin was used as a reference. Each treatment was replicated three times with independent tissue preparations. Different letters and asterisk (*) above standard deviation bars indicate significant differences among means at type I error = 0.05 (LSD test). LSD, least squared difference.

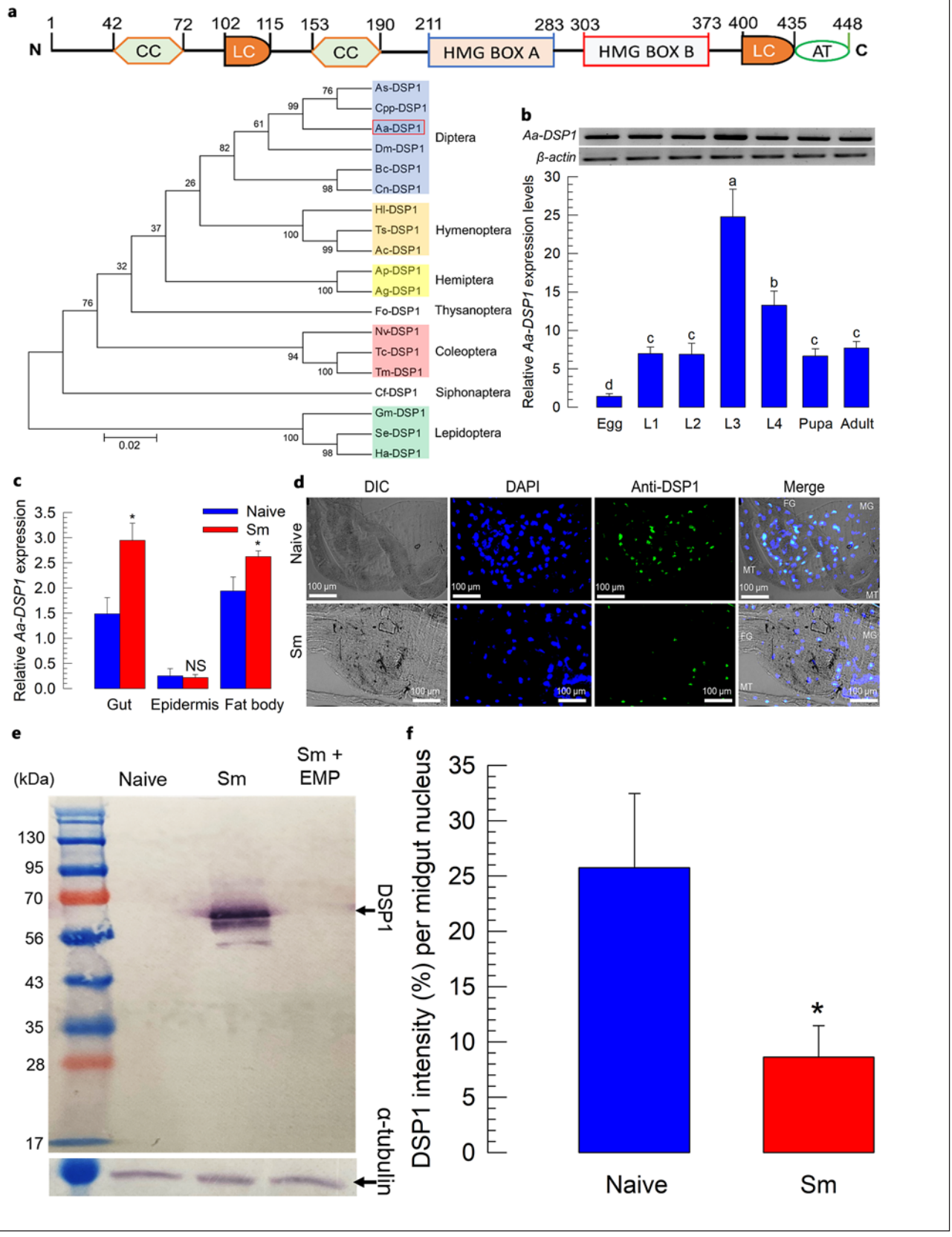

2

(For legend see next page.)

Gut Microbiome

For gut bacterial density analysis, mosquito larvae at L4 instar were dissected under aseptic conditions consisting of cold anaesthetization, surface sanitization by submersion in 70% ethanol, and rinsing in sterile PBS (1 mM, pH 7.4). Entire guts were collected using 70% ethanol-cleaned forceps. DNA samples were isolated using the Wizard Genomic DNA purification kit (Promega, Madison, WI, USA) according to the manufacturer's protocol. Extracted DNA was used as a template in qPCRs with 16S rRNA bacterial primers (online suppl. Table S1). Bacterial 16S rRNA DNA was amplified by RT-qPCR as described above with different annealing temperature 54°C for 30 s. Each measurement used 10 gut samples and was independently replicated three times. Bacterial density was expressed relatively amounts per gut in each control and treatment.

For library construction, DNA was extracted from the gut tissues of the respective dsDuox and dsCON treatments at 24 h postinfection and sent to Macrogen (Seoul, Korea) for sequencing. After performing quality control, qualified samples were proceeded to library construction using the Herculase II fusion DNA polymerase Nextera XT index kit (Illumina, San Diego, CA, USA). For cluster generation, the library was loaded into a flow cell and each fragment was then amplified into distinct, clonal clusters through bridge amplification. Then, the templates were sequenced in Illumina SBS technology. Sequencing data were converted into raw data for analysis. Raw reads were processed with Mothur version 1.43.0 (https://mothur.org/wiki/). Low-quality sequences such as the presence of ambiguous nucleotides, more than eight homopolymers, sequence length lower than the 2.5th percentile, and sequence length higher than the 97.5th percentile were removed. The remaining sequences were pre-clustered to reduce sequencing error (allowing one difference for every 100 bp). Chimeras were removed with VSEARCH (https://github.com/torognes/vsearch). Non-bacterial sequences were removed based on a preliminary classification using the SILVA v132 database (https://www.arb-silva.de/documentation/release-132/). Singletons were removed to avoid operational taxonomic unit (OTU: the operational definition of a species or group of species) overestimation and because of the high sequencing depth of the sampling. Bacterial diversity was estimated with the Chao1, Shannon, and Inverse Simpson indices based on OTU analysis.

Data Analysis

All bioassays were conducted using three independent biological replicates and plotted by mean ± standard deviation using SigmaPlot (Systat Software Inc., San Jose, CA, USA). Means and variances of treatments were compared by the least squared difference test of one-way ANOVA using the PROC GLM of SAS program [31] and discriminated at type I error of 0.05.

Fig. 2. Molecular characterization of *Aa-DSP1*. **a** Domain analysis of Fo-DSP1. Domains were predicted using Prosite (https://prosite.expasy.org/) and SMART protein (http://smart.embl-heidelberg.de/). "CC," "HMG," and "AT" stand for coiled-coil region, high mobility group, and acidic tail, respectively. **b** Expression profile of *Aa-DSP1*. Expression patterns in different developmental stages: egg, first to fourth-instar larvae ("L1–L4"), pupa, and adult. **c** Expression patterns and induction of *Aa-Duox* in response to bacterial challenge in indicated tissues of L4 larvae, including midgut ("Gut"), epidermis, and fat body. L4 larvae were treated with Sm (10^4 CFU/mL) through the feeding assay for 12 h and dissected for studying expression patterns. Each treatment was replicated three times with independent tissue preparations. **d** Nuclear localization of Aa-DSP1 in the midgut epithelium of L4 larvae. Immunofluorescence image was obtained by staining Aa-DSP1 using a specific antibody labeled with FITC. Nuclei were stained with DAPI. "DIC" represents differential interference contrast. **e** A Western blotting showing release of Aa-DSP1 upon bacterial infection into plasma, which was obtained at 12 h after bacterial treatment. EMP (1,000 ppm) was used to treat the larvae along with the bacteria. For each sample preparation, the carcass (excluding gut) of 10 L4 larvae was used and extracted proteins from these samples (20 μg per sample) were separated on SDS-PAGE. **f** Quantitative analysis of Aa-DSP1 intensity in the nucleus of midgut epithelial cell. Each treatment was replicated three times and each replication contained three larvae. Different letters and asterisk (*) above standard deviation bars indicate significant differences among means at type I error = 0.05 (LSD test). LSD, least squared difference.

Results

Aa-Duox and ROS Production in the Midgut of A. albopictus

Interrogation to the transcriptome of *A. albopictus* with the Duox sequence of *D. melanogaster* detected a highly homologous (*E* value = 0.0) orthologue (Fig. 1a). This *Aa-Duox* ORF encoded a 1,508 amino acid sequence with conserved domains found in other Duox genes such as the Ca^{2+}-binding domain and peroxidase domain. This identification was also supported by a phylogenetic analysis indicating that it was clustered with other dipteran Duox genes. *Aa-Duox* was expressed in all developmental stages with the highest expression at the pupal stage (Fig. 1b). In the larval stage, it was expressed in all three tissues (gut, epidermis, and fat body) tested in this study (Fig. 1c). Oral administration of Sm, an entomopathogen, significantly ($p < 0.05$) increased the expression level of *Aa-Duox* in the midgut but not in the epidermis or the fat body. The induction level of *Aa-Duox* expression was highly correlated ($r = 0.85$; $p < 0.01$) with the increase of ROS levels in the gut lumen (Fig. 1d).

Upregulation of Aa-Duox Expression Is Controlled by DSP1 in the Midgut

To explain the upregulation of *Aa-Duox* upon immune challenge, a DAMP molecule in the gut epithelium was investigated. A DSP1 ortholog of *A. albopictus* was predicted from its transcriptome (Fig. 2a). It encoded 448 amino acid residues and possessed two HMG boxes along with both terminal extensions. Phylogenetic analysis in-

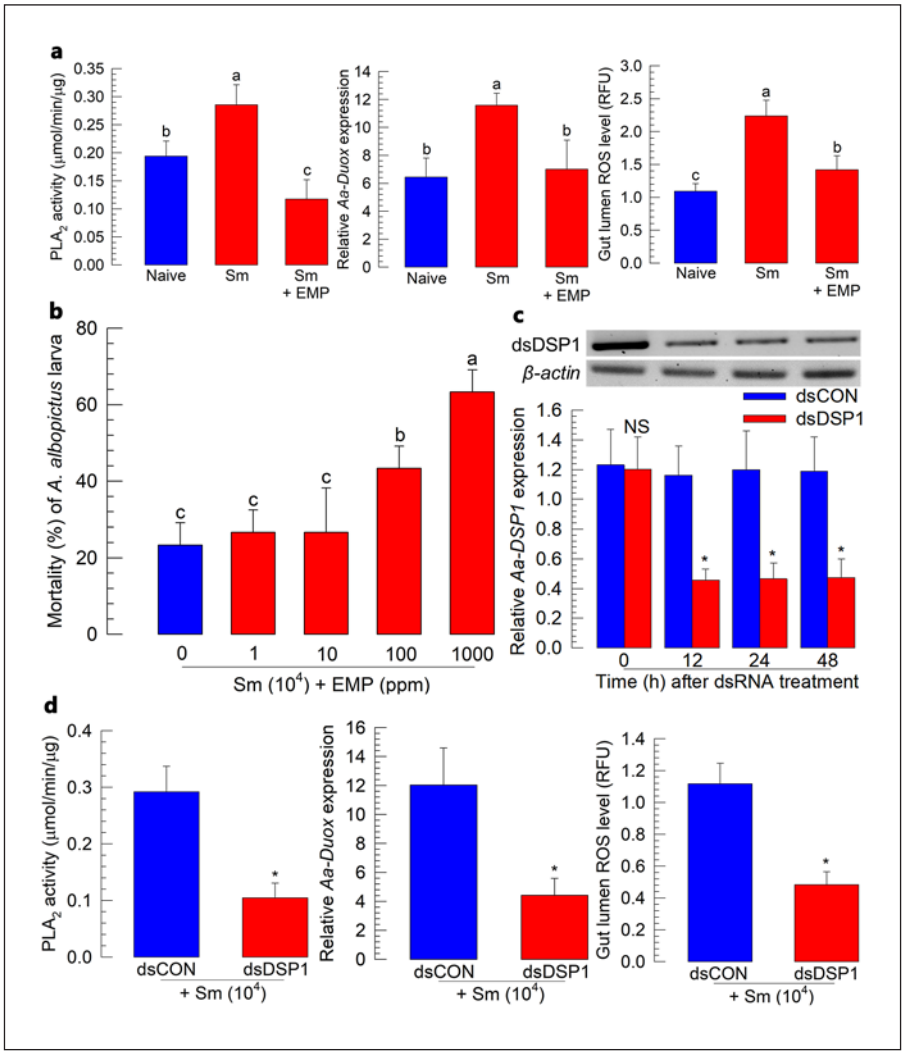

Fig. 3. Influence of DSP1 on the activation of Aa-Duox. **a** Effect of PLA_2 activity induced by Aa-DSP1 release on Aa-Duox expression and ROS production in the gut lumen. **b** Enhancement of bacterial virulence with the addition of EMP against L4 larvae of *A. albopictus*. **c** Effect of RNAi on *Aa-DSP1* expression at different time points in the midgut of L4 larvae. Five microgram of gene-specific dsRNA ("dsDSP1") was added into larval water. **d** Effect of *Aa-DSP1* RNAi on gut PLA_2 activity, *Aa-Duox* expression, and ROS activity in L4 larvae. Bacterial treatment was performed at 12 h after dsRNA injection. At 12 h after bacterial treatment, PLA_2 activity, *Aa-Duox* expression, and ROS production were assessed. Each treatment was replicated three times with independent tissue preparations. Different letters and asterisk (*) above standard deviation bars indicate significant differences among means at type I error = 0.05 (LSD test). LSD, least squared difference.

dicated that *Aa-DSP1* was clustered with other dipteran DSP1 genes. It was expressed in all developmental stages (Fig. 2b). High expression of *Aa-DSP1* was found in late larval stages. Its expression was inducible upon immune challenge, especially in the gut and fat body (Fig. 2c). Aa-DSP1 was localized in the nucleus of the midgut epithelium in the naïve larvae because it overlapped with DAPI (Fig. 2d). Although it was not detected in the plasma of naïve larvae, Aa-DSP1 was released into the plasma in response to bacterial challenge (Fig. 2e). However, EMP, a specific inhibitor for DSP1 [32], prevented the release of Aa-DSP1 from the midgut nucleus (the last lane of Fig. 2e). The release of Aa-DSP1 from the nucleus was supported by the reduction in the protein amount of Aa-DSP1 in the gut epithelium (Fig. 2f) based on cell image ("Sm" treatment in Fig. 2d).

Aa-DSP1 Activates PLA_2 to Upregulate ROS Levels in the Gut Lumen

Bacterial challenge increased PLA_2 enzyme activity, induced *Aa-Duox* expression, and subsequently increased ROS levels in the gut lumen (Fig. 3a). However, these increases were significantly ($p < 0.05$) suppressed after treatment with EMP, known to inhibit Aa-DSP1 release from the gut epithelium. Such immunosuppression induced by EMP increased bacterial virulence to *A. albopictus* larvae in a dose-dependent manner (Fig. 3b). However, EMP alone did not give any toxicity even at 1,000 ppm to the mosquito larvae (online suppl. Fig. S1).

The influence of Aa-DSP1 on PLA_2 activation was assessed by RNAi treatment. Results are shown in Figure 3c. Feeding dsRNA of Aa-DSP1 to mosquito larvae resulted in a significant reduction of *Aa-DSP1* expression

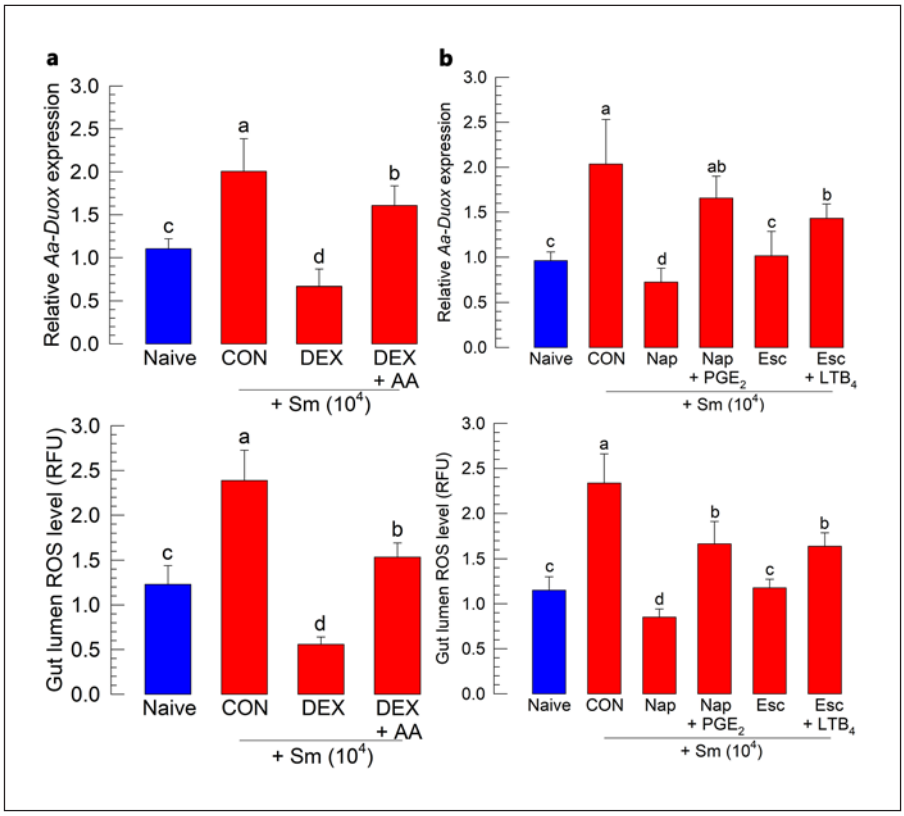

Fig. 4. Influence of PLA_2 inhibitor, COX, and LOX inhibitors on *Aa-Duox* expression and ROS production in the gut. **a** Inhibitory effect of DEX, a PLA_2 inhibitor, on *Aa-Duox* expression and ROS production in L4 larvae. For bacterial challenge, larvae were fed with water containing Sm (10^4 CFU/mL) for 12 h. **b** Influence of NAP, a COX inhibitor, and ESC, a LOX inhibitor, on the expression of *Aa-Duox* and ROS production in L4 larvae. For bacterial challenge, larvae were fed with water containing Sm (10^4 CFU/mL) for 12 h. After 12 h of bacterial treatment, RNA was extracted or intestinal ROS levels were measured. Each treatment was replicated three times and each replication used 15 larvae. Different letters indicate significant differences among means at type I error = 0.05 (LSD test). LSD, least squared difference; COX, cyclooxygenase; LOX, lipoxygenase.

at 12 h posttreatment. Such RNAi treatment prevented the upregulation of PLA_2 activity, which inhibited the upregulation of *Aa-Duox* expression. It also inhibited the subsequent increase of ROS levels in the gut lumen (Fig. 3d).

Eicosanoids Mediate Mosquito Gut Immunity

PLA_2 activity induced by Aa-DSP1 release was further analyzed by investigating specific catalytic products of the enzyme. Results are shown in Figure 4. DEX, an inhibitor of PLA_2, prevented the induction of *Aa-Duox* expression and subsequent ROS increase in the gut lumen (Fig. 4a). However, the addition of AA (a catalytic product of PLA_2) to the group treated with DEX significantly rescued its inhibitory activities. NAP (a cyclooxygenase inhibitor) and ESC (a lipoxygenase inhibitor) showed similar inhibitory activities (Fig. 4b). However, PGE_2 or LTB_4 (eicosanoids) significantly ($p < 0.05$) rescued inhibitory activities of these specific inhibitors. DEX, Nap, or Esc alone did not show any significant influence on the expression of *Aa-Duox* (online suppl. Fig. S2). These results suggest that eicosanoids PG and LT can mediate mosquito gut immunity.

DSP1/PLA_2 Induces Ca^{2+} Signal in the Midgut Epithelium of A. albopictus

Bacterial infection by Sm significantly ($p < 0.05$) increased Ca^{2+} levels in the midgut of *A. albopictus* (Fig. 5a). However, EMP treatment inhibited the induction of the Ca^{2+} signal, suggesting a role of Aa-DSP1. PGE_2 treatment without challenge by Sm induced Ca^{2+} signals in the midgut epithelium, suggesting a PGE_2/Ca^{2+} immune signaling between Aa-DSP1 and PLA_2 (Fig. 5b). Indeed, RNAi specific for *Aa-DSP1* suppressed PGE_2 induction in the gut epithelium (Fig. 5c).

Cyclooxygenase or Lipoxygenase Inhibitors Inhibit Mosquito Gut Immunity and Enhance Virulence of Sm

The influence of gut immunity modulated by eicosanoids was investigated by assessing the virulence of Sm, an entomopathogen, against *A. albopictus*. Mosquito larvae infected with Sm died with a red-colored appearance (Fig. 6a). The insecticidal activity of Sm increased in a dose-dependent manner (Fig. 6b). NAP or ESC treatments significantly ($p < 0.05$) increased larval mortality. However, the addition of PGE_2 or LTB_4 significantly ($p < 0.05$) rescued such lethal effects of NAP and ESC (Fig. 6c).

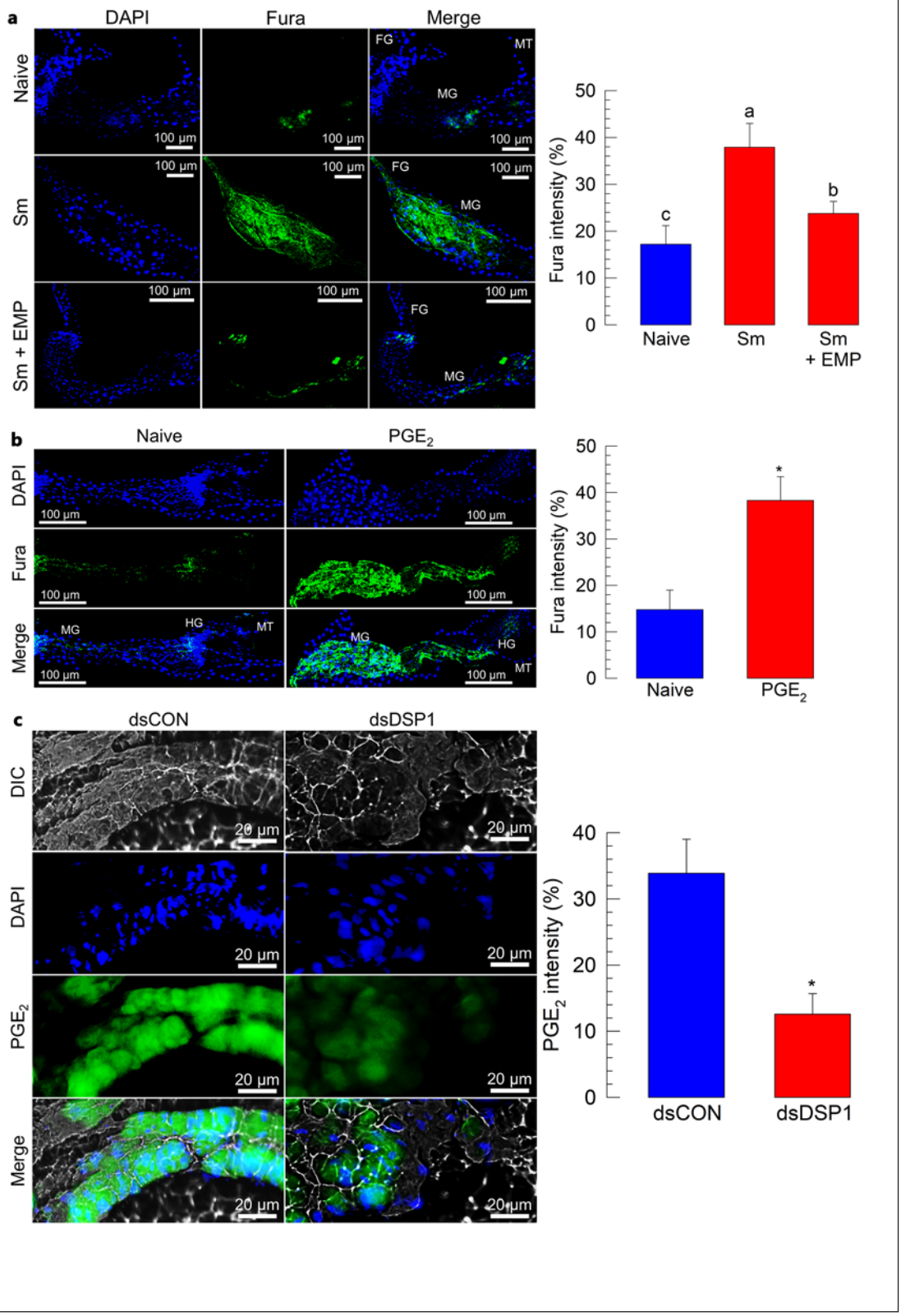

5

(For legend see next page.)

RNAi of Aa-Duox Expression Alters the Microbial Flora in the Mosquito Gut

To support the role of ROS in the gut immunity against the bacterial infection, the expression level of *Aa-Duox* was suppressed by the gene-specific RNAi to decrease ROS level in the gut (Fig. 7). The RNAi treatment suppressed Aa-Duox expression levels, in which more than 80% expression level was reduced at 24 h after the treatment (Fig. 7a). When the bacterial density of the gut lumen was assessed by 16S rRNA amount, the RNAi treatment specific to *Aa-Duox* significantly ($p < 0.05$) elevated the bacterial population (Fig. 7b). However, the bacterial diversity was reduced by the RNAi treatment because the number of bacterial species (= OTUs) decreased along with diversity indices, in which Chao1 is the richness estimate for an OTU definition, the Shannon index takes into account the number and evenness of species, and Inverse Simpson represents the probability that two randomly selected individuals in the habitat will belong to the same species (Fig. 7c). For example, *Pseudomonas*

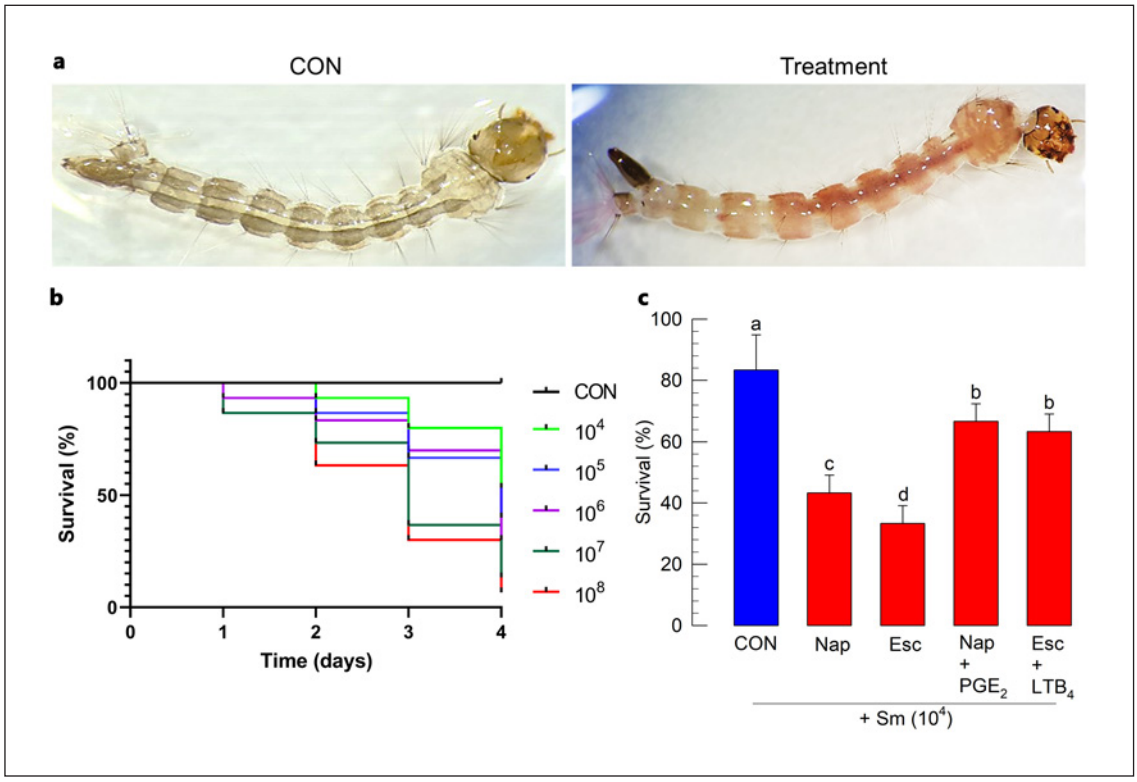

Fig. 6. Influence of eicosanoids on *A. albopictus* survivability against Sm. **a** Larvae infected with Sm showing a red-colored appearance. **b** Pathogenicity of Sm to *A. albopictus* after oral infection. Ten L2 larvae were added to each well of a 48-well plate and monitored for survivorship for 4 days. For bacterial challenge, larvae were fed with water containing Sm (10^4 CFU/mL). **c** Effect of eicosanoid inhibitors on *A. albopictus* survival. NAP (COX inhibitor), ESC (LOX inhibitor), PGE_2, and LTB_4 were added to larval water at a final concentration of 1,000 ppm. Mortality was then checked for 4 days in presence of Sm (10^4). Each treatment consisted of three independent replications and each replication used 10 larvae. Different letters indicate significant differences among means at type I error = 0.05 (LSD test). LSD, least squared difference; COX, cyclooxygenase; LOX, lipoxygenase.

Fig. 5. Induction of Ca^{2+} signal in the midgut epithelium of *A. albopictus* by DSP1/PLA_2. **a** Enhancement of Ca^{2+} level in the midgut after bacterial challenge. For bacterial challenge, larvae were fed with water containing Sm (10^4 CFU/mL) for 12 h. EMP (1,000 ppm) along with bacteria was used for treatment. **b** Induction of Ca^{2+} signal by PGE_2 treatment. Larvae were fed with PGE_2 (1,000 ppm)-treated water for 12 h without bacterial challenge. **c** Suppression of PGE_2 signal in the gut epithelium by RNAi specific to *Aa-DSP1*. PGE_2 was detected with a specific antibody raised in rabbit. Fura-8AM was used to observe Ca^{2+}. Each treatment was replicated three times and each replication contained three larvae. Different letters and asterisk (*) above standard deviation bars indicate significant differences among means at type I error = 0.05 (LSD test). LSD, least squared difference.

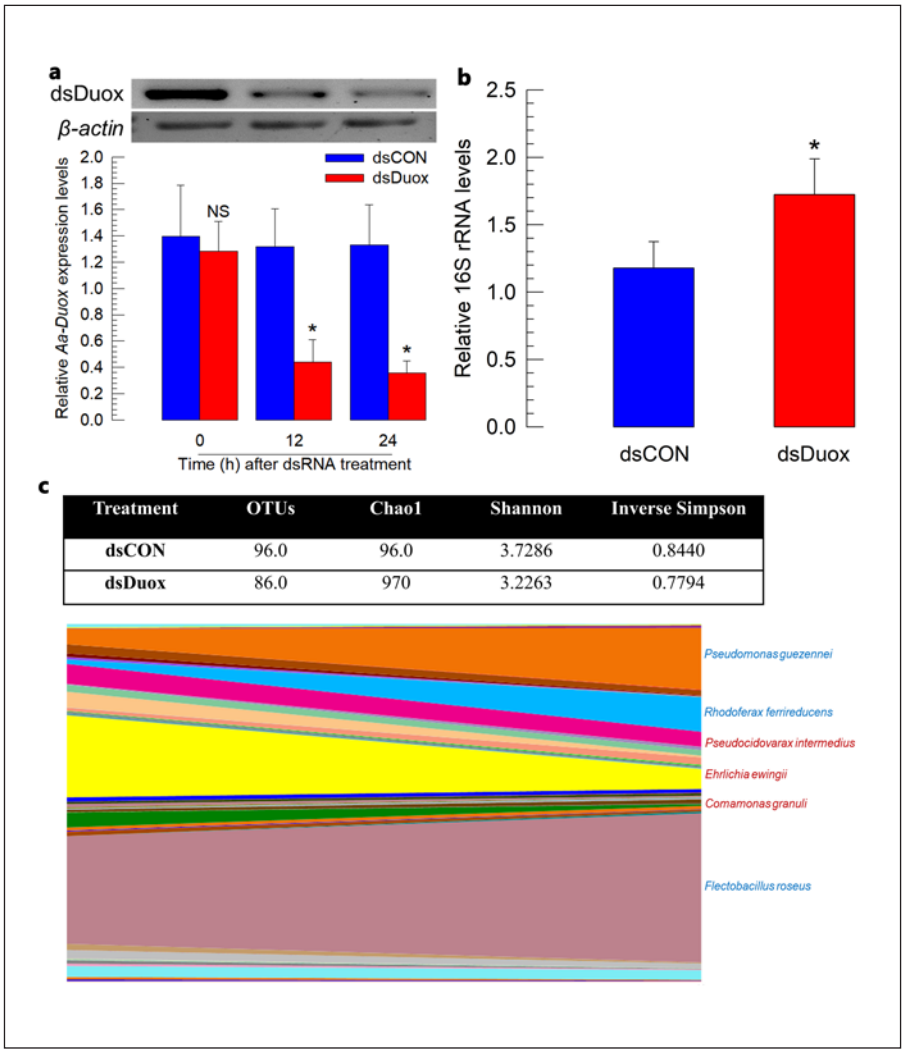

Treatment	OTUs	Chao1	Shannon	Inverse Simpson
dsCON	96.0	96.0	3.7286	0.8440
dsDuox	86.0	970	3.2263	0.7794

Fig. 7. Effect of ROS on gut bacterial flora of *A. albopictus* larvae. dsRNA mediated RNAi of *Aa-Duox* and subsequent influence on intestinal bacterial flora. **a** Suppression of *Aa-Duox* expression by its specific RNAi in L4 larvae. Five microgram of gene-specific dsRNA ("dsDuox") was added to 1 mL of water. **b** Increase of gut bacterial density measured by the relative 16S rRNA level after the RNAi treatment. Each treatment consisted of three independent replications and each replication used 10 larvae. Different letters and asterisk (*) above standard deviation bars indicate significant differences among means at type I error = 0.05 (LSD test). **c** Bacterial community diversity under RNAi treatment specific to *Aa-Duox* in the gut of L4 larvae. Bacterial diversity was presented by Chao1, Shannon, and Inverse Simpson indices based on OTU. Bacterial DNAs were extracted from gut tissues of dsDuox- or dsCON-treated larvae at 24 h PI. Each treatment consisted of three independent replications and each replication used 10 larvae. PI, postinfection. LSD, least squared difference.

guenzennei, *Flectobacillus roseus*, and *Rhodoferax intermedius* were increased, while *Pseudocidovarex intermedius*, *Ehrlichia ewingii*, and *Comamonas granuli* were decreased in their densities.

Discussion

Pathogens are recognized in the hemocoel where PRRs discriminate against specific pathogens and trigger immune responses via immune mediators [33]. In mosquitoes transmitting *Plasmodium* parasites, ookinetes penetrating gut epithelium may encounter both free and membrane-bound PRRs in the hemocoel, which would promote downstream immune signaling or directly induce immune responses [34]. PRRs can activate immune deficiency pathway [35] and other major immune signaling pathways such as Toll, Jun-N-terminal kinase, and Janus kinase/signal transducers and activators of transcription [36, 37]. With respect to gut immunity, the gut epithelium in *Drosophila* is immunocompetent and upon enteric infection initiates innate immune responses via the immune deficiency signal pathway, mediating AMP production as well as the pathway related to Duox activation to produce ROS [38–40]. Alternatively, gut immunity is suppressed by Caudal [9] and Nubbin [7] to preserve commensal and symbiotic microbes. However, a clear pathogen recognition in the gut lumen where numerous microbes reside remained elusive. Thus, this study tested the role of HMGB1-like DSP1 as another direct damage signal to the gut epithelium in response to a bacterial pathogen.

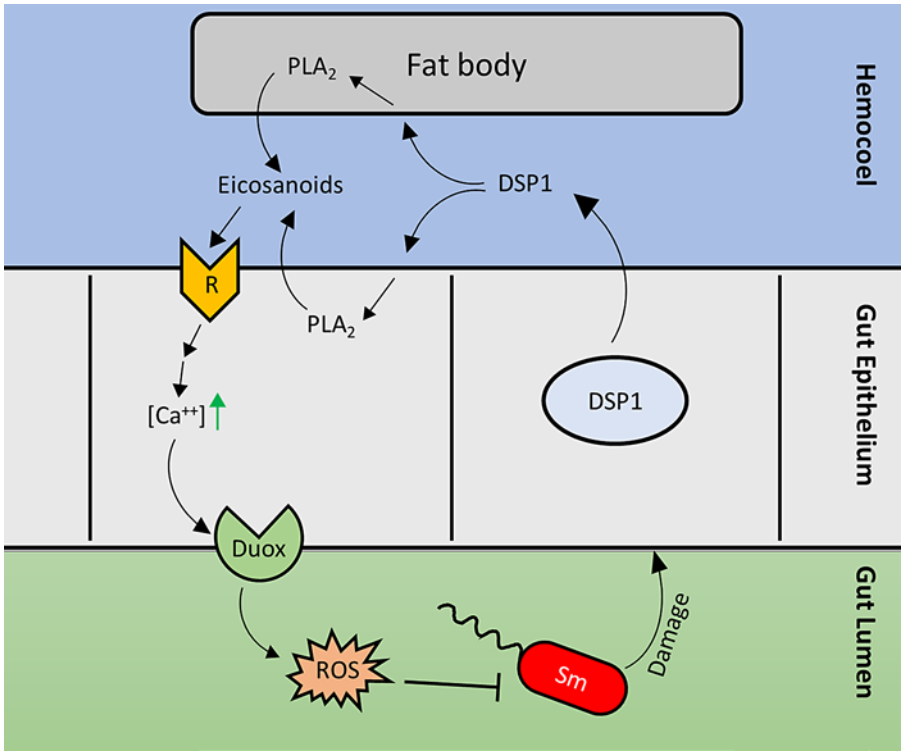

Fig. 8. A model of eicosanoids mediating DSP1/Ca^{2+}/Duox signaling pathway in the midgut epithelium of *A. albopictus* in response to oral infection by Sm. Upon infection by Sm, damage-associated pattern molecule ("DSP1") is released from the gut epithelium into the hemocoel. Released DSP1 activates "PLA_2" to synthesize eicosanoids in the gut epithelium or fat body. Autocrine/paracrine eicosanoids bind to their respective receptors ("R") to induce intercellular Ca^{2+} levels. The upregulated Ca^{2+} then activates "Duox" to produce "ROS" and finally defend against Sm.

Oral infection by Sm caused significant mortality of *A. albopictus* larvae in the present study. Nehme et al. [39] have shown that Sm can resist the systemic immune response elicited by AMPs in *Drosophila* due to the presence of lipopolysaccharide-O-antigen. However, when ingested, flies died at a rate dependent on the bacterial load in the food. ROS and AMPs produced from the insect gut are effective in defending against microbial infections [41]. Our current study showed that ROS production induced by eicosanoids was effective in defending against the bacteria in *A. albopictus*. This suggests that ROS can act as a potent immune effector against bacterial infection in the mosquito, using a microbiome analysis, This was supported by a change in bacterial flora using a microbiome analysis after RNAi specific to Aa-Duox expression. This suggests the defense role of ROS in the gut against the pathogen infection of Sm.

ROS production in *A. albopictus* was positively correlated with the expression level of *Aa-Duox*. Duox catalyzes NADPH-dependent oxidation to produce hydrogen peroxide and subsequent ROS. *Aa-Duox* expression was observed in all developmental stages, with a high expression level at the pupal stage of naïve mosquitoes. The physiological significance of such high expression of *Aa-Duox* at the pupal stage is unknown. Interestingly, another mosquito species, *Anopheles stephensi*, also exhibits a high expression of its *Duox* gene during the pupal stage [42]. In that study, RNAi of this *Duox* gene in *An. stephensi* suppressed its parasite *Plasmodium* development, suggesting a defensive role of Duox activity in the mosquito gut against pathogen infection. Indeed, *Aa-Duox* expression was inducible by Sm infection. In addition to the immune defense role of Duox in mosquitoes, Duox activity has a function of maintaining microbial homeostasis in mosquitoes. Infection by *Beauveria bassiana*, an entomopathogenic fungus, can cause dysbiosis of *An. stephensi* gut microbiota, with a significant increase in gut bacterial load and a significant decrease in bacterial diversity via downregulation of *Duox* expression [43].

The induction of *Aa-Duox* expression was caused by the release of Aa-DSP1. RNAi of *Aa-DSP1* expression prevented the induction of *Aa-Duox* expression, which failed to upregulate ROS level in the gut lumen in response to bacterial infection by Sm. In addition, treatment with EMP, a specific inhibitor, prevented Aa-DSP1 release into plasma. EMP can bind to DSP1 of *Spodoptera exigua* and prevents its translocation out of cells [32]. Bacterial infection by Sm was accompanied by ROS generation in the present study, suggesting that a damage

signal might have occurred in the gut epithelium. In vertebrates, HMGB1 acts as a damage signal after it is released from the nucleus into the plasma where it interacts with particular receptors such as Toll-like receptors to activate immune responses [25, 44]. DSP1, an ortholog of vertebrate HMGB1, has been found in *S. exigua* [22]. It is known to be secreted from hemocytes or fat bodies in response to immune challenges1 [22]. This secreted DSP1 can interact with specific Toll receptors and activate PLA_2 to induce cellular and humoral immune responses [32]. In the current study, DSP1 signal was mostly found in the nucleus of the gut epithelium of naive *A. albopictus* larvae. After infection by Sm through oral feeding, DSP1 was observed in the plasma of infected larvae. However, it was not detected in the plasma of naïve larvae. This delineated that DSP1 in the nucleus of the gut epithelium was released into the hemolymph after Sm infection-mediated gut injury.

The release of Aa-DSP1 increased PLA_2 activity in *A. albopictus* presumably to synthesize eicosanoids. Indeed, both eicosanoids PGE_2 and LTB_4 were effective in inducing *Aa-Duox* expression, subsequently elevating ROS levels in the gut lumen. In *Anopheles gambiae* (another mosquito), specific leukotriene called lipoxin A4 plays a role in immune priming after the mosquito midgut was infected by *Plasmodium* by elevating PGE_2 levels in the midgut epithelium to attract hemocytes to the infection foci. In the current study, PGE_2 was observed in the gut epithelium of *A. albopictus*. Its signal intensity was increased after bacterial infection by Sm. However, any interruption of Aa-DSP1 release failed to increase PGE_2 levels in the midgut, suggesting that PLA_2 was activated by Aa-DSP1 to produce PGE_2. This was supported by the finding that treatment with eicosanoid biosynthesis inhibitors is known to prevent the induction of *Aa-Duox* expression and subsequent ROS generation, whereas the addition of PGE_2 or LTB_4 considerably reversed such inhibition.

The enzymatic activity of Duox, which is controlled by Ca^{2+} signals in the *Drosophila* model, is thought to upregulate ROS generation after pathogen detection [14]. Although bacterial-derived uracil has been recognized as a pathogen signal, pathogen identification by the gut epithelium remains unknown [15]. To explain this, a general damage signal molecule, HMGB1-like DSP1, was identified as a pathogen-associated molecule in the present study. It could elicit gut immunity in *A. albopictus* against bacterial infection. On the other hand, nonpathogenic commensal microbes occasionally induce dysregulation of gut homeostasis by stimulating ROS. In this case, another DAMP molecule triggers the immune response. This is well demonstrated in a null mutant *Drosophila* in a PRR gene, *PGRP-SG*, which facilitates overgrowth of a commensal bacterium, *Lactobacillus plantarum*, and the resulting excess lactic acid acting as a DAMP to produce ROS from the gut epithelium [45].

After bacterial infection, Ca^{2+} signal in the gut epithelium was significantly increased. PGE_2 alone mediated the increase of Ca^{2+} signal in the gut epithelium, leading to elevated ROS levels in the gut lumen of *A. albopictus*. A PGE_2 receptor has been identified in *S. exigua* [46]. Upon activation, this receptor stimulated two secondary messengers, in which cAMP was induced earlier. It was required for the subsequent induction of the Ca^{2+} signal [21]. Sajjadian and Kim [17] have added a role of cAMP in inducing *Se-Duox* expression via cAMP-responsive element-binding protein in response to PGE_2 in the gut epithelium. These results suggest a working model (Fig. 8) of a gut immunity signal pathway from bacterial infection to ROS generation using the DSP1/PLA_2/Ca^{2+}/Duox signaling pathway. The role of eicosanoid in gut immunity was further supported by a pathogenicity bioassay, in which the virulence of Sm against mosquito larvae was enhanced by the addition of eicosanoid biosynthesis inhibitors.

Statement of Ethics

No approval of studies involving animals was required.

Conflict of Interest Statement

The authors have no conflicts of interest relevant to this study to disclose.

Funding Sources

This work was supported by a grant (No. 2022R1A2B5B0300-1792) of the National Research Foundation (NRF) funded by the Ministry of Science, ICT and Future Planning, Republic of Korea. This study was also funded by a research grant from Andong National University to Y.K.

Author Contributions

Yonggyun Kim and Shabbir Ahmed designed the experiments for this work. Shabbir Ahmed and Seyedeh Minoo Sajjadian collected the samples to perform the experiments. Shabbir Ahmed

and Seyedeh Minoo Sajjadian analyzed the data. Yonggyun Kim and Shabbir Ahmed wrote and edited the manuscript. Yonggyun Kim managed the funding. All the authors read and approved the manuscript.

Data Availability Statement

All data generated or analyzed during this study are included in this article and its online supplementary material files. Further inquiries can be directed to the corresponding author.

References

1 Medlock JM, Hansford KM, Schaffner F, Versteirt V, Hendrickx G, Zeller H, et al. A review of the invasive mosquitoes in Europe: ecology, public health risks, and control options. Vector Borne Zoonotic Dis. 2012 Jun;12(6):435–47.
2 Anyanwu EC, Ehiri JE, Kanu I, Merrick J. Health effects of long-term exposure to insecticide-treated mosquito nets in the control of malaria in endemic regions, revised. ScientificWorldJournal. 2006 Dec 15;6:1631–41.
3 Berg H. Global status of DDT and its alternatives for use in vector control to prevent disease. Environ Health Perspect. 2009 Nov;117(11):1656–63.
4 Wang S, Jacobs-Lorena M. Genetic approaches to interfere with malaria transmission by vector mosquitoes. Trends Biotechnol. 2013 Feb;31(3):185–93.
5 Paupy C, Delatte H, Bagny L, Corbel V, Fontenille D. *Aedes albopictus*, an arbovirus vector: from the darkness to the light. Microbes Infect. 2009 Dec;11(14–15):1177–85.
6 Van den Hurk AF, Nicholson J, Beebe NW, Davis J, Muzari OM, Russell RC, et al. Ten years of the tiger: *Aedes albopictus* presence in Australia since its discovery in the torres strait in 2005. One Health. 2016 Feb;24(2):19–24.
7 Lindberg BG, Tang X, Dantoft W, Gohel P, Esfahani SS, Lindvall JM, et al. Nubbin isoform antagonism governs *Drosophila* intestinal immune homeostasis. PLoS Pathog. 2018 Mar;14(3):e1006936.
8 Zhang LJ, Gallo RL. Antimicrobial peptides. Curr Biol. 2016 Jan;26(1):R14–9.
9 Lee KA, Kim B, Bhin J, Kim DH, You H, Kim EK, et al. Bacterial uracil modulates *Drosophila* DUOX-dependent gut immunity via hedgehog-induced signaling endosomes. Cell Host Microbe. 2015 Feb;17(2):191–204.
10 Marra A, Hanson MA, Kondo S, Erkosar B, Lemaitre B. *Drosophila* antimicrobial peptides and lysozymes regulate gut microbiota composition and abundance. mBio. 2021 Aug;12(4):e0082421.
11 Kuraishi T, Hori A, Kurata S. Host-microbe interactions in the gut of *Drosophila melanogaster*. Front Physiol. 2013 Dec;4:375.
12 Engel P, Moran NA. The gut microbiota of insects: diversity in structure and function. FEMS Microbiol Rev. 2013 Sep;37(5):699–735.
13 Oliveira JHM, Goncalves RLS, Lara FA, Dias FA, Gandara ACP, Menna-Barreto RFS, et al. Blood meal-derived heme decreases ROS levels in the midgut of *Aedes aegypti* and allows proliferation of intestinal microbiota. PLoS Pathog. 2011 Mar;7(3):e1001320.
14 Ha EM, Lee KA, Park SH, Kim SH, Nam HJ, Lee HY, et al. Regulation of DUOX by the Gαq-phospholipase Cβ-Ca2+ pathway in *Drosophila* gut immunity. Dev Cell. 2009 Mar;16(3):386–97.
15 Lee KA, Kim SH, Kim EK, Ha EM, You H, Kim B, et al. Bacterial-derived uracil as a modulator of mucosal immunity and gut-microbe homeostasis in *Drosophila*. Cell. 2013 May;153(4):797–811.
16 Sajjadian SM, Kim Y. Dual oxidase-derived reactive oxygen species against *Bacillus thuringiensis* and its suppression by eicosanoid biosynthesis inhibitors. Front Microbiol. 2020 Mar;11:528.
17 Sajjadian SM, Kim Y. PGE2 upregulates gene expression of dual oxidase in a lepidopteran insect midgut via cAMP signalling pathway. Open Biol. 2020 Oct;10(10):200197.
18 Kim Y, Ahmed S, Stanley D, An C. Eicosanoid-mediated immunity in insects. Dev Comp Immunol. 2018 Jun;83:130–43.
19 Park J, Kim Y. Change in hemocyte populations of the beet armyworm, *Spodoptera exigua*, in response to bacterial infection and eicosanoid mediation. Korean J Appl Entomol. 2012 Dec;51(4):349–56.
20 Barletta ABF, Trisnadi N, Ramirez JL, Barillas-Mury C. Mosquito midgut prostaglandin release establishes systemic immune priming. iScience. 2019 Sep;19:54–62.
21 Ahmed S, Kim Y. PGE2 mediates hemocyte-spreading behavior by activating aquaporin via cAMP and rearranging actin cytoskeleton via Ca2. Dev Comp Immunol. 2021 Dec;125:104230.
22 Mollah MMI, Choi HW, Yeam I, Lee JM, Kim Y. Salicylic acid, a plant hormone, suppresses phytophagous insect immune response by interrupting HMG-Like DSP1. Front Physiol. 2021 Oct;12:744272.
23 Decoville M, Giacomello E, Leng M, Locker D. DSP1, an HMG-like protein, is involved in the regulation of homeotic genes. Genetics. 2001 Jan;157(1):237–44.
24 Choi HW, Manohar M, Manosalva P, Tian M, Moreau M, Klessig DF. Activation of plant innate immunity by extracellular high mobility group box 3 and its inhibition by salicylic acid. PLoS Pathog. 2016 Mar;12(3):e1005518.
25 Roh JS, Sohn DH. Damage-associated molecular patterns in inflammatory diseases. Immune Netw. 2018 Aug;18(4):e27.
26 Lehming N, Thanos D, Brickman JM, Ma J, Maniatis T, Ptashne M. An HMG-like protein that can switch a transcriptional activator to a repressor. Nature. 1994 Sep;371(6493):175–9.
27 Mollah MMI, Kim Y. HMGB1-like dorsal switch protein 1 of the mealworm, *Tenebrio molitor*, acts as a damage-associated molecular pattern. Arch Insect Biochem Physiol. 2021 Jul;107(3):e21795.
28 Livak KJ, Schmittgen TD. Analysis of relative gene expression data using real-time quantitative PCR and the 2(-Delta Delta C(T)) method. Methods. 2001 Dec;25(4):402–8.
29 Vatanparast MD, Ahmed S, Herrero S, Kim Y. A non-venomous sPLA2 of a lepidopteran insect: its physiological functions in development and immunity. Dev Comp Immunol. 2018 Dec;89:83–92.
30 Bradford MM. A rapid and sensitive method for the quantitation of microgram quantities of protein utilizing the principle of protein-dye binding. Anal Biochem. 1976 May;72:248–54.
31 SAS Institute Inc. SAS/STAT user's guide. Cary, NC, USA: SAS Institute; 1989.
32 Mollah MMI, Ahmed S, Kim Y. Immune mediation of HMG-like DSP1 via Toll-Spätzle pathway and its specific inhibition by salicylic acid analogs. PLoS Pathog. 2021 Mar;17(3):e1009467.
33 Gillespie JP, Kanost MR, Trenczek T. Biological mediators of insect immunity. Annu Rev Entomol. 1997;42:611–43.
34 Saraiva RG, Kang S, Simões ML, Angleró-Rodríguez YI, Dimopoulos G. Mosquito gut antiparasitic and antiviral immunity. Dev Comp Immunol. 2016 Nov;64:53–64.
35 Dong Y, Das S, Cirimotich C, Souza-Neto JA, McLean KJ, Dimopoulos G. Engineered *Anopheles* immunity to *Plasmodium* infection. PLoS Pathog. 2011 Dec;7(12):e1002458.
36 Christophides GK, Vlachou D, Kafatos FC. Comparative and functional genomics of the innate immune system in the malaria vector *Anopheles gambiae*. Immunol Rev. 2004 Apr;198:127–48.
37 Garver LS, de Almeida Oliveira G, Barillas-Mury C. The JNK pathway is a key mediator of *Anopheles gambiae* antiplasmodial immunity. PLoS Pathog. 2013 Sep;9(9):e1003622.
38 Liehl P, Blight M, Vodovar N, Boccard F, Lemaitre B. Prevalence of local immune response against oral infection in a *Drosophila/Pseudomonas* infection model. PLoS Pathog. 2006 Jun;2(6):e56.
39 Nehme NT, Liégeois S, Kele B, Giammarinaro P, Pradel E, Hoffmann JA, et al. A model of bacterial intestinal infections in *Drosophila melanogaster*. PLoS Pathog. 2007 Nov;3(11):e173.

40 Ryu JH, Kim SH, Lee HY, Bai JY, Nam YD, Bae JW, et al. Innate immune homeostasis by the homeobox gene caudal and commensal-gut mutualism in *Drosophila*. Science. 2008 Feb;319(5864):777–82.
41 Lee KA, Lee WJ. *Drosophila* as a model for intestinal dysbiosis and chronic inflammatory diseases. Dev Comp Immunol. 2014 Jan; 42(1):102–10.
42 Kakani P, Kajla M, Choudhury TP, Gupta L, Kumar S. *Anopheles stephensi* dual oxidase silencing activates the thioester-containing protein 1 pathway to suppress plasmodium development. J Innate Immun. 2019 Mar; 11(6):496–505.
43 Wei G, Lai Y, Wang G, Chen H, Li F, Wang S. Insect pathogenic fungus interacts with the gut microbiota to accelerate mosquito mortality. Proc Natl Acad Sci U S A. 2017 Jun; 114(23):5994–9.
44 Tsung A, Klune JR, Zhang X, Jeyabalan G, Cao Z, Peng X, et al. HMGB1 release induced by liver ischemia involves toll-like receptor 4-dependent reactive oxygen species production and calcium-mediated signaling. J Exp Med. 2007 Nov;204(12):2913–23.
45 Iatsenko I, Boquete JP, Lemaitre B. Microbiota-derived lactate activates production of reactive oxygen species by the intestinal NADPH oxidase Nox and shortens *Drosophila* lifespan. Immunity. 2018 Nov;49(5):929–e5.
46 Kim Y, Ahmed S, Al Baki MA, Kumar S, Kim K, Park Y, et al. Deletion mutant of PGE2 receptor using CRISPR-Cas9 exhibits larval immunosuppression and adult infertility in a lepidopteran insect, *Spodoptera exigua*. Dev Comp Immunol. 2020 Oct;111:103743.